UPPSALA
UNIVERSITET

Digital Comprehensive Summaries of Uppsala Dissertations from the Faculty of Science and Technology 389

Neutron Scattering at 96 MeV

ANGELICA ÖHRN

ACTA
UNIVERSITATIS
UPSALIENSIS
UPPSALA
2008

ISSN 1651-6214
ISBN 978-91-554-7079-1
urn:nbn:se:uu:diva-8425

Dissertation presented at Uppsala University to be publicly examined in Häggsalen, Ångströmlaboratoriet, Lägerhyddsvägen 1, Uppsala, Friday, February 29, 2008 at 10:15 for the degree of Doctor of Philosophy. The examination will be conducted in English.

Abstract
Öhrn, A. 2008. Neutron Scattering at 96 MeV. Acta Universitatis Upsaliensis. *Digital Comprehensive Summaries of Uppsala Dissertations from the Faculty of Science and Technology* 389. 52 pp. Uppsala. ISBN 978-91-554-7079-1.

Data on elastic scattering of 96 MeV neutrons from ^{56}Fe, ^{89}Y and ^{208}Pb in the angular interval 10-70° are presented. The previously published data on ^{208}Pb have been extended, as a new method has been developed to obtain additional information at the most forward angles. The results are compared with phenomenological and microscopic optical potentials. The theory predictions are in general in good agreement with the experimental data.

A study of the deviation of the zero-degree cross section from Wick's limit has been performed. The data on ^{208}Pb are in agreement with Wick's limit, while those on lighter nuclei overshoot the limit significantly.

A novel analysis method has been developed to obtain the inelastic neutron emission cross sections from the existing ^{56}Fe data. The method is based on folding a trial spectrum with the response of the detector setup. The data cover the angular interval 26-65° and an excitation energy range of 0-45 MeV, ranges hitherto not studied. The results are compared with nuclear model predictions and found to be in good agreement with the experimental data.

Keywords: neutron, elastic scattering, inelastic scattering, differential cross section, optical model potential, Wick's limit, angular distribution, pre-equilibrium

Angelica Öhrn, Department of Physics and Astronomy, Division of Applied Nuclear Physics, Box 525, Uppsala University, SE-751 20 Uppsala, Sweden

ISSN 1651-6214
ISBN 978-91-554-7079-1
urn:nbn:se:uu:diva-8425 (http://urn.kb.se/resolve?urn=urn:nbn:se:uu:diva-8425)

Till de viktigaste personerna i mitt liv,
min man Calle och vår son Alexander.

List of Papers

This thesis is based on the following papers, which are referred to in the text by their Roman numerals.

I J. Klug, J. Blomgren, A. Ataç, B. Bergenwall, A. Hildebrand, C. Johansson, P. Mermod, L. Nilsson, S. Pomp, U. Tippawan, K. Elmgren, N. Olsson, A.V. Prokofiev, P.-U. Renberg, P. Nadel-Turonski, S. Dangtip, P. Phansuke, M. Österlund, C. Le Brun, J.F. Lecolley, F.R. Lecolley, M. Louvel, N. Marie-Noury, C. Schweitzer, Ph. Eudes, F. Haddad, C. Lebrun, A.J. Koning, and X. Ledoux, (2003) Elastic neutron scattering at 96 MeV from ^{12}C and ^{208}Pb. *Phys. Rev. C*, 68:064605, http://link.aps.org/abstract/PRC/v68/e064605.

II P. Mermod, J. Blomgren, C. Johansson, A. Öhrn, M. Österlund, S. Pomp, B. Bergenwall, J. Klug, L. Nilsson, N. Olsson, U. Tippawan, P. Nadel-Turonski, O. Jonsson, A. Prokofiev, P.-U. Renberg, Y. Maeda, H. Sakai, A. Tamii, K. Amos, R. Crespo, and A. Moro, (2006) 95 MeV neutron scattering on hydrogen, deuterium, carbon, and oxygen. *Phys. Rev. C*, 74:054002, http://link.aps.org/abstract/PRC/v74/e054002.

III A. Öhrn, J. Blomgren, P. Andersson, A. Ataç, C. Gustavsson, J. Klug, P. Mermod, S. Pomp, P. Wolniewicz, M. Österlund, L. Nilsson, B. Bergenwall, K. Elmgren, N. Olsson, U. Tippawan, S. Dangtip, P. Phansuke, P. Nadel-Turonski, O. Jonsson, A. Prokofiev, P.-U. Renberg, V. Blideanu, C. Le Brun, J.F. Lecolley, F.R. Lecolley, M. Louvel, N. Marie-Noury, C. Schweitzer, Ph. Eudes, F. Haddad, C. Lebrun, E. Bauge, J.P. Delaroche, M. Girod, X. Ledoux, K. Amos, S. Karataglidis, R. Crespo, and W. Haider, (2008) Elastic scattering of 96 MeV neutrons from iron, yttrium and lead. Accepted for publication in *Phys. Rev. C*.

IV A. Öhrn, J. Blomgren, A. Ataç, C. Gustavsson, J. Klug, P. Mermod, L. Nilsson, S. Pomp, M. Österlund, B. Bergenwall, K. Elmgren, N. Olsson, U. Tippawan, S. Dangtip, P. Phansuke, P. Nadel-Turonski, O. Jonsson, A. Prokofiev, P.-U. Renberg, P. Ascher, V. Blideanu, C. Le Brun, J.F. Lecolley, F.R. Lecolley, M. Louvel, N. Marie-Noury, C. Schweitzer, Ph. Eudes, F. Haddad, C. Lebrun, X. Ledoux, M. Blann, S. Chiba, H. Duarte, C. Kalbach, A. Koning, and Y. Watanabe, (2008) Inelastic neutron scattering cross sections at 96 MeV on iron, in manuscript.

Reprints were made with permission from the American Physical Society. The author changed family name from Hildebrand to Öhrn in June 2005.

Comments on my contribution

Paper I was written while I was still a rather fresh PhD student. My contribution is modest and consists of partly writing the code for calculations of effective solid angles for the experimental setup. Later, I have, however, re-analysed the data on ^{208}Pb, see Paper III and IV. My contribution to Paper II is mainly participation during the experiment. The results from Paper I and II have also been used for the normalization of the data in Paper III and IV. Concerning Paper III and IV, I have been responsible for the main part of the work, from participating in the experiments, analysing the data and developing new analysis methods to writing the manuscripts.

Contents

1. Introduction

"Kärnfysik? Oj, det låter svårt."
Vanlig kommentar

1.1 The present work

Does the world outside the academic society need neutron data? The answer is yes. Handling of spent nuclear fuel, fast neutron cancer therapy and studies of failure in aircraft electronics due to cosmic-ray neutrons are a few examples of this. Moreover, neutron data are also of great importance in research in fundamental physics as they reveal important properties of nuclei.

In this thesis new neutron data are presented, a work performed within the experimental neutron reactions programme at the Division of Applied Nuclear Physics, Department of Physics and Astronomy at Uppsala University. Experiments on elastic neutron scattering from carbon, oxygen, iron, yttrium and lead have been performed and analysed. The existing analysis routines from Paper I have been extended to obtain additional information at the most forward angles. This has also lead to a re-analysis of the already existing data on elastic neutron scattering from ^{208}Pb. In addition to this, a study of the deviation from Wick's limit has been performed.

It has been possible to extend the analysis of the existing data on carbon, iron, yttrium and lead to extract information on inelastic neutron scattering in an angular and excitation-energy range hitherto not studied. The method as such and first results on ^{56}Fe will be presented here.

The outline of the thesis is the following: In this introduction, the importance of the new neutron data are discussed as well as a review on the neutron data situation in the nuclear data libraries of today. Theoretical aspects of neutron scattering and an introduction to the optical model are treated in chapter 2. This is followed by an overview of the neutron facility at the The Svedberg Laboratory and the SCANDAL setup in chapter 3. The measurements on elastic and inelastic scattering are discussed in chapter 4 and 5, respectively. Finally, a summary and conclusions are given in chapter 6.

1.2 Neutron data

The nuclear data libraries of today are rather limited for neutron energies above 20 MeV. There are high-quality neutron total cross section data on a series of nuclei up to about 600 MeV [1], and (n,p) data in the forward angular range at modest excitation energies are available up to about 300 MeV for a rather large number of nuclei [2, 3].

Extensive measurements of the np scattering cross section have been performed. For a list of data sets, see Refs. [4, 5]. The number of measurements on neutron elastic scattering from nuclei heavier than $A = 6$ is, however, small. An extensive data set on elastic neutron scattering at 96 MeV has been produced at The Svedberg Laboratory in Uppsala (see Paper I, II and [6]), but apart from this, only three experiments above 30 MeV have produced data with an energy resolution adequate for resolving individual nuclear states; an experiment at MSU at 30 and 40 MeV [7, 8], one at UC Davis at 65 MeV [9, 10] and another one at LAMPF from 65 to 255 MeV [11]. Experiments at 55, 65 and 75 MeV have been performed at TIARA, Japan Atomic Energy Research Institute [12, 13], with energy resolutions in the $10 - 20$ MeV range. Also available are a few measurements in the $0 - 30^\circ$ range, between 80 and 350 MeV, all with energy resolutions of 15 MeV or worse [14, 15, 16, 17, 18]. At small angles, this poor energy resolution is not a serious drawback, as elastic scattering dominates heavily. At larger angles, however, such a resolution makes the data very difficult to interpret. An overview of the neutron elastic scattering experiments is given in Table 1.1, where studied nuclei, neutron energies, energy resolutions and angular ranges are shown.

For inelastic neutron scattering (n,n'x), the data base is even more limited. Except the measurements presented in this thesis, there is only one experiment reported above 30 MeV, i.e., data at 65 MeV from UC Davis on iron, tin and lead [19]. In that work, data in the $13 - 32^\circ$ and $20 - 65$ MeV angular and neutron emission energy ranges were presented.

Recently, an experimental effort to provide (n,n'x) data with essentially complete coverage of neutron emission energy has been undertaken at the The Svedberg Laboratory by a Caen-Uppsala collaboration, as part of the EUROTRANS [20] project. In that experiment, part of the SCANDAL [21] setup, which was also used for the measurements presented here, was used, together with the dedicated converter system CLODIA [22, 23, 24] for neutron detection above 50 MeV. For lower energies, a time-of-flight based system was utilized. Two targets were studied, lead and iron. Preliminary results have been presented in a PhD thesis [22] and at a conference [23].

This scarcity of neutron data has motivated the scattering measurements at 96 MeV presented in this thesis. As scattering experiments are large time and money consumers, the main focus on how to improve the neutron data situation must be on developing theoretical models rather than systematic measurements for a large number of nuclei. The obvious nuclei to study are the magic or semi-magic ones, i.e., ^{12}C, ^{16}O, ^{40}Ca, ^{90}Zr and ^{208}Pb. Carbon, oxygen and calcium are all of direct medical and dosimetric relevance. Iron, zirconium and lead are considered to be important materials in future transmutation facilites (see next Section).

Table 1.1: Neutron elastic scattering experiments with neutron energies $E_n \geq 30$ MeV.

Reference	Target	Energy (MeV)	Resolution (MeV at FWHM)	Angular range (°)
[7, 8]	Ca, Si	30, 40	0.15	15–140
[12, 13]	C, Si, Fe, Zr, Pb	55, 65, 75	10–20	2–57
[10]	C, Si, Ca, Fe, Sn, Pb	65	2.7	6–50
[14]	Al, Cu, Pb	84	30	2–25
[11]	C, Ca, Pb	65–225	4.5	7–23
[15]	Li, Be, C, Al ,Cu, Cd, Pb, U	96	24	1–29
[16]	Li, Be, C, N, O, Al, Cu, Cd, Pb	136	27	0–20
[17]	C, Al, Cu, Cd, Pb	155	60	3–30
[18]	C, Al, Cu Sn, Pb	350	15	1–20
Paper I,II	C, O	96	3.7	10–70
Present exp.	Fe, Y, Pb	96	3.7	10–70

1.3 Applications

As mentioned in the previous section, neutron data are not only of academic interest, but have several interesting applications, for example handling of spent nuclear fuel, fast neutron therapy and in studies of failure of electronics due to cosmic-ray neutron radiation.

The spent fuel from nuclear power plants contains, besides the uranium isotopes ^{235}U and ^{238}U, large amounts of fission products, having roughly half the mass and atomic numbers of uranium, and elements heavier than uranium (transuranium elements, TRU) formed by neutron capture reactions in heavy elements followed by beta decay. Immediately after the removal of the fuel assemblies from the reactor core their radioactivity is very high and dominated by the decay of the fission fragments, which have on average relatively short half lifes. The fuel assemblies are therefore stored for several decades in specially designed intermediate storage facilities. The half lifes of some of the produced transuranium elements are, however, very long (of the order of 100 000 years or more), and the spent fuel must be kept separated from the biosphere over very long time periods.

These circumstances have lead to two methods of taking care of the spent nuclear fuel:

- Wait for the decay (typically 100 000 years) keeping the material incapsulated.
- Convert the long-lived components of the material to stable or short-lived elements using nuclear transmutation.

The first alternative has in many countries, including Sweden, lead to plans on geological repositories several hundred meters below ground level.

The second alternative is often referred to as transmutation. In the public debate, transmutation has been synonymous with accelerator-driven systems (ADS) for incineration of nuclear waste. This is, however, not the only possibility being investigated. Plutonium, could for example be burnt in the already existing critical reactors, thermal light water reactors (LWR) or fast reactors. Burning plutonium in a critical reactor requires separation from uranium, to prevent further build up of plutonium. The other TRUs require fast neutron spectra to be burnt efficiently. The situation is, however, different than for plutonium. An important fundamental property of uranium and also of plutonium is their relatively high fraction of beta-delayed neutrons, which makes it possible to run a critical reactor in a safe and controlled way. The other TRUs have significantly lower fractions of beta-delayed neutrons which would make an ADS, run in sub-critical mode, an attractive alternative.

Transmuting minor actinides into stable or less long-lived isotopes is today possible at laboratory scale, i.e., the challenge is not to find the fundamen-

tal physical properties for transmutation, but to develop a working system of industrial scale.

In a sub-critical reactor, neutrons are constantly fed to the core by an external source. An example of an external source, which has attracted a lot of interest, is neutron production using a spallation target. Protons with energies of about 1 GeV impinge on a target, for example lead or bismuth, and neutron of energies ranging from $0-1$ GeV are produced. This means that in the reactor core of an ADS there will be neutrons of energies much higher than in the reactors of today. In order to design the core properly, neutron data covering this whole energy range are needed. As mentioned earlier, the nuclear data libraries of today have limited data sets above 20 MeV, whereas transmutation would benefit from nuclear data also above this energy.

Four elements have attracted special interest for nuclear data measurements; lead as spallation/cooling material, iron for shielding and construction, uranium as fuel and zirconium as fuel cladding. The data presented in this thesis cover three of these four requests. The deformed shape of the ^{238}U nucleus makes measurement of elastic neutron scattering difficult, mainly because of problems of resolving the ground state. In our experiments, we have used ^{89}Y instead of ^{90}Zr simply because the desired amount of ^{90}Zr was not possible to obtain. Instead of using natural zirconium, which contains several isotopes none of abundance above about 50%, a monoisotopic target (^{89}Y) was preferred.

Whether transmutation is a viable answer to the problems related to the handling of spent nuclear fuel remains an open question [25]. There are still numerous problems that need to be solved. Even if transmutation of spent nuclear fuel would be a reality in the future, a geological storage would still be necessary, but the safety and time conditions might not have to be as stringent as they are formulated today.

Other applications of fast neutrons that would benefit from improved knowledge of neutron reactions are fast neutron cancer therapy and studies of electronics failure induced by cosmic-ray neutrons. Fast neutrons have sometimes given good results when conventional radiation therapy has not been succesful [26, 27]. Neutrons themselves make no damage to the tissue, but if they induce a nuclear reaction, the emitted charged products interact with the surrounding matter. This means that a fundamental understanding of the effects in tissue due to neutrons requires knowledge of two stages. First the probability for neutrons to create charged particles must be known and also such details as particle type, energy, direction, etc. Second, the biologic effect of the secondary particle must be known. Today, the second stage above is reasonably well known, whereas the first step, i.e., knowledge of the cross sections of the different nuclear reactions that produce charged particles needs improvement.

About half the dose in human tissue due to fast neutrons comes from proton recoils in neutron-proton (n,p) scattering, 10-15 % from nuclear recoils due to

neutron scattering and the remaining 35-40 % from neutron-induced emission of light ions, i.e., protons, deuterons, tritons, ^{3}He and α-particles. Modern neutron therapy beams extend up to 70 MeV, while most evaluated data bases cover the energy region up to 20 MeV, as mentioned above. This makes it difficult to correctly estimate the dose given, and to plan and optimize the therapy. Hence, the needs of data for cancer therapy partly coincide in energy with those for transmutation applications.

In the last decades, it has become evident that electronics in airplanes can fail due to irradiation of cosmic-ray neutrons [28, 29]. One effect is that a neutron can induce a nuclear reaction in the silicon substrate of a memory device, which could cause a memory flip. This is usually called single-event upset (SEU) and is obviously not wanted. As computer technologies is going towards smaller and smaller device geometries, this leads to a larger sensitivity to particle irradiation and therefore, this problem can nowadays be found in computers at sea level as well. For normal computer usage, this is usually not an obstacle, but for computer systems which require high reliability this is certainly a serious matter. Also here data on neutron scattering is beneficial for the understanding on how this problem arises. For a more complete review on the nuclear data needs, see Ref. [29].

Elastic neutron scattering is also of general importance for the applications described above. Scattering data and data on total cross sections are needed for the development of the optical model, a powerfool tool to predict cross sections for which no measurements exist, see Chapter 2. This makes elastic neutron scattering measurements much more important than they would be if they were only useful for, e.g., calculations of the spatial distribution of neutrons in a core.

2. Theory

2.1 Elastic scattering

The differential cross sections for elastic scattering of neutrons from nuclei have characteristics that are common to a wide range of target nuclei, and to neutron energies spanning over several orders of magnitude. They show a general trend of falling off with increasing scattering angle, and this behaviour is modulated by an oscillating function with pronounced minima and maxima. This resembles a familiar problem in optics: the diffraction of light by an opaque disque or a small slit, see Fig 2.1. In the optics case, it is the edges that produce a series of maxima and minima. The first minimum occurs at an angle $\theta \sim \lambda/R$ from the direction of the incident wave (λ is the wavelength and R is the disk radius), the succeeding minima are roughly equally spaced and the maxima are of steadily and substantially decreasing intensity. The intensity of the minima are equal to zero, see Fig 2.2. In the case of nuclear scattering, the nucleus is the analogue of the disk. The surface of a nucleus is, however, not sharp but diffuse and therefore the minima of the elastic scattering cross sections do not reach zero.

There are some important features of the optical diffraction that are analogous to the scattering of neutrons:

- The incident wave is represented by a plane wave, while the scattered wave fronts are spherical. Since the total energy content of any expanding spherical wave front cannot vary, its intensity per unit area must decrease as r^{-2} and its amplitude as r^{-1}.
- Along the surface of any spherical scattered wave front, the diffraction is responsible for the variation in intensity of the radiation. Therefore, the intensity depends on the angle of observation.
- A detector placed at any point far from the object records waves that are superpositions of the incident and the scattered waves.

Using this information it is possible to derive an expression for the elastic scattering cross section, starting with the Schrödinger equation,

$$\nabla^2\Psi + \frac{2m}{\hbar^2}(E-U)\Psi = 0, \tag{2.1}$$

where m is the reduced mass, E, the energy of the incident particle and U the potential depth. For a review of a derivation, see for example Refs. [30, 31].

The form of the nuclear potential can be parametrized and inserted in the Schrödinger equation. By solving the Schrödinger equation for an incident particle, predictions can be made for cross sections. This is often referred to as the optical model and is the subject of the next section.

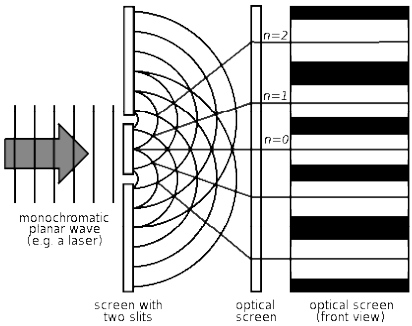

Figure 2.1: Diffraction of plane waves from two slits. On the optical screen, the minima and maxima from the diffraction can be observed [32].

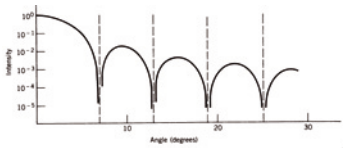

Figure 2.2: Diffraction pattern of light scattered from a circular disk. In this example, the diameter of the disk is approximately ten times the wavelength [30].

2.1.1 The optical model

The interaction between a nucleon and a nucleus is of fundamental importance in nuclear physics. It determines the elastic and inelastic scattering of nucleons by nuclei, as well as the behaviour of the nucleon channels in nuclear reactions.

A study of an incident nucleon interacting with a target nucleus requires the solution of a many-body equation. The system can, however, be approximated by considering two bodies interacting via a complex mean-field potential. This so called optical model potential (OMP) is an important ingredient in calculations of cross sections, e.g., elastic and inelastic scattering, (p,n) and (n,p) reactions. In other words, a good global optical model is a powerful tool for predicting observables at energies and for nuclides for which no measurements exist.

There are basically two ways of determining the optical potential, the phenomenological and the theoretical. The former starts from a physically rea-

sonable form of the potential and its parameters are adjusted by fits to experimental data. For the theoretical approach, often referred to as the microscopic optical potential, the effective potential is established theoretically, which will be described later in this section. This means that the phenomenological and the microscopic optical potentials are different, not only in their formulation but also in their intent. The phenomenological approach is a data-driven formulation, for which data are required in advance to define the parameter values of the potential. Microscopically formed optical potentials are predetermined, and their success or failure in reproducing measured data reflects on whatever inadequacies there may be in the underlying facets of their formulation.

For the phenomenological optical model, the basic form of the potential can be written as

$$U(r) = V(r) + iW(r). \tag{2.2}$$

The potential must have a complex part part to allow for non-elastic scattering, i.e., the potential must be partly absorptive. The potential consists of a central term (V), a spin-orbit term (SO) and a Coulomb term (C),

$$U(r) = -U_V(r) + U_{SO}(r) + U_C(r), \tag{2.3}$$

expressed in terms of their real and imaginary parts. The components are expected to roughly follow the shape of the matter distribution. A common shape is the Woods-Saxon form factor

$$f(r) = f(r,R,a) = [1 + exp(\frac{r-R}{a})]^{-1}, \tag{2.4}$$

where r_0 in $R = r_0 A^{1/3}$ is the nuclear radius parameter and a is the diffuseness parameter.

To describe the non-elastic processes in a quantatively better way, a surface term is added to the central term. This term is added because the Pauli exclusion principle prevents the tightly bound orbitals in the nuclear interior to participate in the absorption of incident neutrons.

As mentioned earlier in the text, the parameters of the phenomenological optical model potential are determined by fitting the predicted cross sections to experimental data. There are basically three types of phenomenological OMPs [33]; (i) a "best-fit" OMP, representing a potential for one nucleus at one single incident energy, (ii) a local OMP, representing a potential for one nucleus in an energy region, and (iii) a global OMP, covering both a mass region and an energy region. The best fit to experimental data is given by the best-fit potentials, but the results of the obtained parameters can display values that make them unsuitable for use in other energy regions and for prediction of cross sections. Another risk with the best-fit method is that the obtained parameters can have unphysical values. With the global model, it is possible to obtain an average description of the nuclear interactions as a function of mass

and energy. The global model assumes that a smooth A dependence of the Woods-Saxon form factor gives a good description of the matter distribution in the nucleus over the whole mass range. This is a generalization and is therefore not perfectly true, as nuclei with filled shells are more tightly bound than nuclei with unfilled shells. When studying a particular nucleus, the local OMP might, however, be a better choice.

A combination of these three approaches can, however, be succesful. The best-fit OMP can be used to obtain start values in a fitting procedure, while the local and global OMP can be used to keep the parameters within physically reasonable bounds.

For the microscopic optical model, as mentioned earlier in the text, an effective nuclear potential is established where the nucleons are not treated individually. This effective potential can be determined by for example folding of the nucleon-nucleon effective interaction with the matter density distribution. The matter density can be determined by different methods, from phenomenological parametrizations to Hartree-Fock based folding of all the involved nucleon-nucleon interactions. Subsequently, the scattering from this effective potential is computed.

2.1.2 Wick's limit

Using the optical theorem it is possible to derive an expression which establishes a lower limit of the differential elastic cross section at 0° if the total cross section is known. This is often referred to as Wick's limit [34, 35]. Using the notation from Ref. [31], a derivation of Wick's limit will follow here.

The total cross section is the sum of elastic and absorption cross sections. If the incident particle is uncharged this is

$$\sigma_{tot} = \sigma_{el} + \sigma_{abs}. \tag{2.5}$$

Expressed in terms of partial wave matrix elements, Eq. 2.5 can be written as:

$$\begin{aligned} \sigma_{tot} &= \pi\lambda\!\!\!^{-2} \sum_\ell (2\ell+1)[|1-\eta_\ell|^2 + 1 - |\eta_\ell|^2] \\ &= 2\pi\lambda\!\!\!^{-2} \sum_\ell (2\ell+1)[1 - Re\eta_\ell] \end{aligned} \tag{2.6}$$

Since $|\eta_\ell \leq 1|$, maximum of the total cross section is obtained for $\eta_\ell = -1$, and is composed of elastic scattering only.

For elastic scattering, the scattering amplitude is

$$f(\theta) = \frac{1}{2ik} \sum_\ell (2\ell+1)[\eta_\ell - 1] P_\ell(cos\theta) \tag{2.7}$$

and at 0° where $cos\theta = 1$

$$f(\theta = 0) = \frac{1}{2ik} \sum_\ell (2\ell+1)[\eta_\ell - 1] \tag{2.8}$$

Comparison with Eq. 2.6 gives the optical theorem which relates the total cross section to the imaginary part of the $\theta = 0$ elastic scattering amplitude

$$\sigma_{tot} = 4\pi\lambda\!\!\!^{-} Imf(\theta = 0). \tag{2.9}$$

Since the elastic differential cross section is $d\sigma_{el}/d\Omega = |f(\theta)|^2$, the optical theorem 2.9 gives rise to *Wick's inequality*

$$\sigma_{tot} \leq 4\pi\lambda\!\!\!^{-} (\frac{d\sigma}{d\Omega})^{1/2}. \tag{2.10}$$

2.2 Reaction mechanisms

A simple way of characterizing nuclear reactions is by dividing them into types where the classification is determined by for example time scales or number of intranuclear interactions. Direct reactions are governed by short reaction times ($\sim 10^{-22}$ s) and on the other extreme, there are the compound nuclear processes with reaction times of $\sim 10^{-16}$ s. In between, at intermediate time scales, the so called pre-equilibrium (or pre-compound) reactions can be found. This can also be expressed in terms of the number of intranuclear interactions; one or two for direct reactions, a few for pre-equilibrium reactions and many for compound reactions. From this follows that the coupling between the incident and outgoing channels weakens with the number of collisions, and that the statistical nature of the nuclear reaction theories used to describe these processes becomes more dominant.

In a direct reaction, the incident particle interacts primarily at the surface of the target, via individual nucleon-nucleon interactions. Pre-equilibrium reactions represent an intermediate process, in which a few interactions take place in the nucleus. Data from such a measurement display less structure than direct reactions, but more than for compound reactions.

In a compound reaction, which is a typical reaction when the incident particle energy is rather low (a few MeV or less), an incident particle is interacting with the nucleus forming a compound nucleus, which subsequently decays, typically by neutron emission. It is mainly governed by the total energy of the system as the compound nucleus has no "memories" of the formation process.

In (n,n'x) experiments all these three processes take place. This can be seen when studying a neutron-energy (or excitation-energy) spectrum. The direct reactions correspond to the highest neutron-emission energies, pre-equilibrium reactions to the intermediate energies and the compound reactions to the lowest energies. An illustration of this is shown in Figs. 2.3 and 2.4.

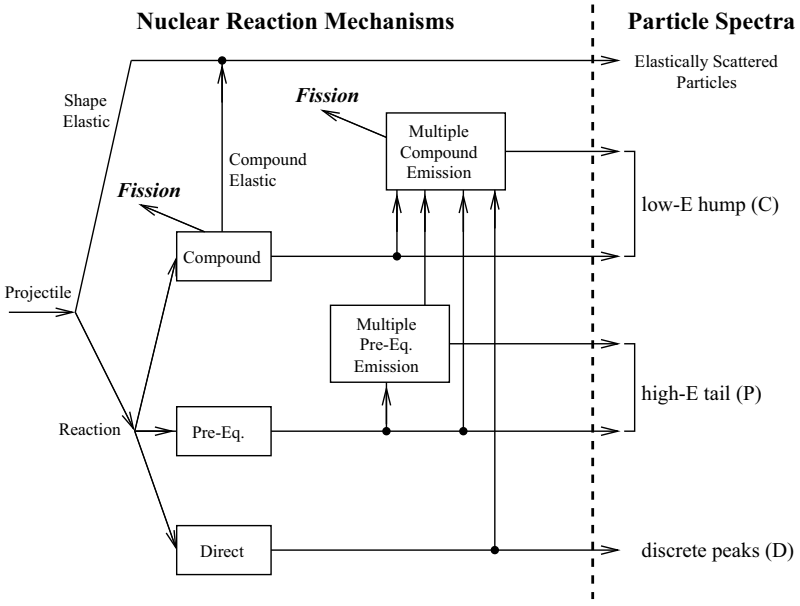

Figure 2.3: The role of direct, pre-equilibrium and compound processes in the description of a nuclear reaction and the outgoing particle spectra. *C* corresponds to compound processes, *P* to pre-equilibrium and *D* to direct processes [36].

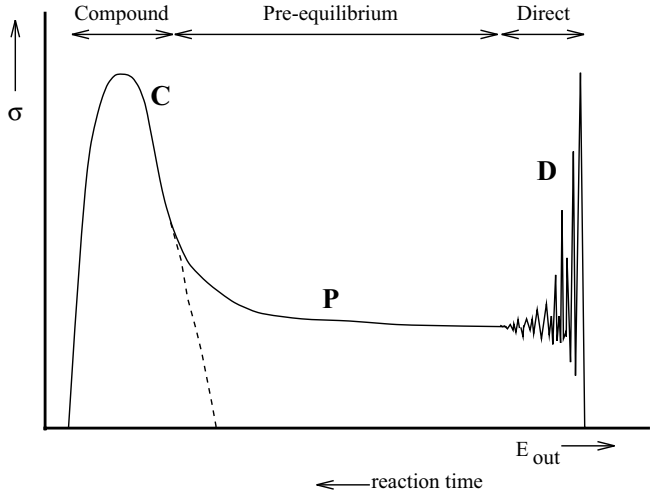

Figure 2.4: Schematical drawing of an outgoing particle spectrum. The energy regions to which direct, pre-equilibrium and compound mechanisms contribute are indicated [36].

3. Measurements of neutron scattering at 96 MeV

3.1 The Svedberg Laboratory

The experiments performed for this thesis have been carried out at the neutron facility at the The Svedberg Laboratory at Uppsala University. The facility has been described in detail in Ref. [21]. Detailed information is also given in Paper I and therefore only the principles of the neutron facility will be described here.

The The Svedberg Laboratory (TSL) offers a monoenergetic neutron beam, covering the energy range 20-180 MeV. An overview of the neutron beam facility is shown in Fig 3.1. Neutrons were produced by protons impinging on a lithium target. After the lithium target, the proton beam was bent into a well-shielded beam dump. The resulting neutron spectrum consisted of a peak at the incident proton energy and a low-energy neutron tail, which was suppressed by time-of-flight techniques. The neutron beam was defined by a system of three collimators, which have given the beam an approximate diameter of 10 cm and a neutron yield of $2.5 \cdot 10^6$ s^{-1} over the whole beam area. The neutron beam was dumped in a tunnel about 10 m downstream of the experimental position. Neutron monitoring was performed by a fission counter, a thin film breakdown counter (TFBC), and the integrated proton beam current from the proton beam dump.

The neutron beam facility has recently been rebuilt. The neutron production target has been moved closer to the experimental area, resulting in an increased neutron intensity of the beam. This will facilitate scattering measurements at 180 MeV in reasonable data taking times.

3.2 The SCANDAL setup

The experimental setup SCANDAL (SCAttered Nucleon Detection AssembLy) was used to detect the scattered neutrons, see Fig 3.2. A detailed description of SCANDAL is given in Ref. [21] and therefore, only an overwiev will be given here. The detection of neutrons is based on conversion to protons and detection of the recoil protons. The setup consists of two identical arms placed on each side of the beam, covering the angular ranges 10–50° and 30–70°. Each arm has a 2 mm thick veto scintillator for fast rejection of charged-particles, a 10 mm thick neutron-proton converter scintillator, a 2

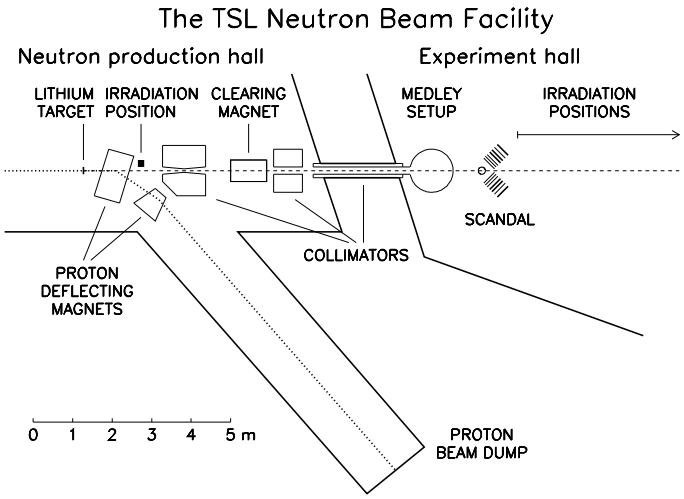

Figure 3.1: Overview of the TSL neutron beam facility.

mm thick ΔE plastic scintillator for triggering, two drift chambers for proton tracking, another 2 mm thick ΔE plastic scintillator which is also part of the trigger, and an array of CsI detectors (12 on each arm) for energy determination of the recoil protons produced in the converter by *np* scattering. The trigger, when detecting neutrons, is defined by a coincidence of the two trigger scintillators, with the front detector acting as a veto. It is also possible to run SCANDAL in proton mode, by changing the veto detector to accept charged particles. The total energy resolution of the individual CsI crystals is different, and on average 3.7 MeV (FWHM), see Ref. [21].

3.3 Experimental procedure

Details on the experimental and analysis procedure are presented in Paper I, II and III and will only be briefly covered here. The experiments were carried out in different runs of about one week each. Each experimental week begun with a calibration measurement in which a CH_2 target was placed in the neutron beam and recoil protons from *np* scattering were detected. After calibration, the SCANDAL setup was changed to neutron detection mode in which the veto scintillator signals are used for charged-particle rejection. Four scattering

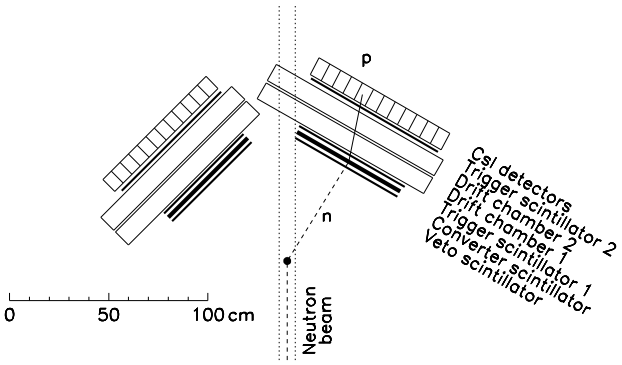

Figure 3.2: Schematic layout of the SCANDAL setup. A typical event is indicated.

targets in form of cylinders were used, natural iron, yttrium, radiogenic lead and carbon, the latter one used to provide data for normalization. Background data were recorded after removing the scattering cylinder from the setup.

3.4 Data analysis

In this section, the analysis routines will be described and the differences on how to treat the data for elastic as well as inelastic scattering will be highlighted.

The data were analyzed offline event-by-event. As a first step, the time information from the drift chambers was converted to positions. This information was used to calculate the angular information, the detector hit positions and the particle trajectories. The coordinates were also used to trace the protons, which in turn were used to establish the hit positions in the CsI detectors and the conversion points in the converter scintillator.

Each CsI detector was calibrated individually with *np* data from the calibration runs. Two calibration peaks in each CsI detector were identified; the pedestal channel corresponding to zero-energy deposition in the detector, and the *np* scattering peak. A linear relationship was assumed between pulse height (PH) and deposited energy. The energy of the *np* peak was obtained by calculating the energy loss of the proton through the detector setup from the target to the CsI in question. The centroid channel was determined by fitting a gaussian to the *np* peak.

Each plastic scintillator has two PM tubes attached to one of the longer horizontal sides. They were calibrated by choosing a narrow, central section of the scintillator, i.e., where the distance is approximately the same to both PM tubes and where it can be assumed that these detect half the light each. Also for the plastic scintillators, the pedestal channel and the proton peak were used as calibration points. The total deposited energy in the plastic scintillators (ΔE) was obtained by adding the contribution from the two PM tubes. The shape of the plastic scintillators give rise to a geometric effect, i.e., protons with the same energy yield slightly different ΔE signals depending on where they hit the detector. The deviation from the expected ΔE value was mapped over the detectors as a function of the location in the scintillator, both horizontally and vertically, and could subsequently be compensated for.

To obtain the correct energy loss throughout the whole detector setup, the energy losses in materials where the proton is not detected, such as detector wrapping, drift chamber foils, drift chamber gas and air, were calculated.

Finally, the total energy of the charged particle was calculated as the sum of the different contributions from the detectors and other materials. This resulted in excitation-energy spectra for the different angles in the laboratory system related to the position of the CsI crystal in which the proton was stopped.

As a second stage of the analysis, gates on the positions, energies and conversion angles were applied. Protons were separated from other charged particles, mostly deuterons originating from the converter scintillator, by a $\Delta E - E$ technique.

To reject events from the low-energy tail of the neutron spectrum, a time-of-flight (TOF) cut was used. The TOF was defined as the time difference between the first trigger detector and a signal from the cyclotron radiofrequency system. For the elastic scattering measurement, this information is not important, as a low-energy neutron in the beam cannot induce emission of a full-energy neutron from the scattering target. For the inelastic scattering measurement this cut is of importance for the determination of the experimental response function, see chapter 5.

Scatter plots with the horizontal and vertical hit positions in the CsIs were constructed. In these scatter plots, two-dimensional cuts were applied in order to select the accepted hit area. Since the energy determination for events where a proton passes through more than one CsI detector is very poor, due to large straggling effects in CsI wrapping materials, it was important that the position cuts were set in such a way that the protons were completely stopped in a single detector.

In the early experiments using the SCANDAL setup for elastic scattering measurements, (see Paper I, II and Ref. [6]), each CsI crystal defined an angular bin. In Paper III, however, the CsI area for the crystals at the most forward angles, where the statistics allow such a procedure, has been divided into two areas to obtain additional data points and to improve the angular resolution at

forward angles. This resulted in 36 angular bins for ^{56}Fe, 32 bins for ^{89}Y and 30 for ^{208}Pb. The statistics were better for the iron experiment and therefore allowed more CsI detector hit areas to be split.

For the inelastic scattering measurement, bins were merged to allow for more statistics at especially the largest angles. This resulted in five angular bins for the ^{56}Fe measurement. See chapter 5 for more details.

Since the converter scintillator contains both carbon and hydrogen, neutrons can be converted to protons by the ^{12}C(n,p) reaction instead of the desired *np* scattering, i.e., H(n,p). The Q-value for the ^{12}C(n,p) reaction is -12.6 MeV, meaning that at forward angles an energy cut is sufficient to distinguish between the two reactions. At conversion angles larger than about 20° the proton energies from the two processes overlap and it cannot be decided from which reaction the proton originates. Therefore, an opening angle criterion was set, demanding that the conversion angle be less than 10°. The procedure described above was also applied to the background data.

Up to this point, the data reduction was performed event-by-event. Subsequently, the data were stored in excitation-energy histograms, one for each angular bin. Background data were subtracted from the signal spectra after normalization to the same neutron fluence and taking dead time into consideration. The corresponding operations were also performed to produce variance histograms, to be used for estimation of the statistical errors.

4. Elastic scattering of 96 MeV neutrons from iron, yttrium and lead

In the previous chapter, the analysis of the data was described up to the point where background-subtracted data were stored in excitation-energy histograms, one for each angular bin. In this chapter, the extraction of cross sections for elastic scattering will be discussed. Details as well as tables of the results are presented in Paper I, II and III.

4.1 Cross section calculations

To obtain the number of elastic scattering events at each angle, gaussians were fitted to the ground state peak and the lowest excited states, and subsequently, the areas of the gaussians were calculated.

The variance of the number of elastic scattering events was extracted by applying this method also to the variance histograms. At large angles, the fitting procedure described above could not be used due to poor statistics. For those angles, the ground state yield was extracted by integration, within limits determined by visual inspection.

The number of neutrons in the beam was given by either the fission counter (TFBC) or the integrated proton beam current. The number of target nuclei was calculated from the weight and volume of the scattering target. The solid angles for protons detected in the CsI crystals are individual for each crystal depending on the distance to the target and the size of the accepted detection area. A computer code was developed to calculate the solid angles as well as the average neutron scattering angle for each bin, see Paper I.

Since the energy resolution is different for individual CsI crystals, the low-energy continuum originating from the ^{7}Li(p,n) reaction contributes differently to the full-energy *np* peaks at different angles and hence to the ground state peaks in the excitation-energy spectra. This contribution, which is a function of the peak width [37] has been determined using experimental neutron spectra for the ^{7}Li(p,n) reaction measured by Byrd and Sailor [38]. Correction factors for this effect were used when calculating the cross section. The correction is typically around 3 % and always less than 6 %.

The proton detection efficiency has contributions from the efficiencies of each drift chamber plane, the efficiency of selecting the correct drift chamber

wire in multiple-hit events and the CsI efficiency. The total proton detection efficiency has been measured to 0.64 ± 0.10.

The absolute scale of the cross sections was given by measuring the number of neutrons in the beam using the TFBC monitor. The TFBC has, however, an uncertainty of more than 10 % for the absolute number of neutrons and therefore further normalization was required. In Paper I a new normalization method was introduced, using the known data on the total cross section and the reaction cross section to calculate the total elastic cross section to which our data were normalized. For carbon, the normalization uncertainty was estimated to 3 %. Measuring relative to carbon has been adopted by us as a secondary standard for normalization of our data. We estimate the normalization procedure to have an uncertainty of about 5 %.

Since extended targets have been used for the present experiments, corrections for neutron attenuation and multiple scattering were necessary. These corrections have been performed using a Monte Carlo code [39]. As input to the code, an angular distribution in the laboratory system was given, in this case the experimental data obtained with SCANDAL. After conversion to the c.m. system and calculation of the attenuation, the code simulated the experiment. The aim of the program was to find a distribution that, when used as input for the simulation, resulted in an output reproducing the measured angular distribution. For the new dataset on ^{208}Pb this turned out not to be a good method as the angular distribution showed such prominent structure that the code could not succesfully describe it. Instead a simulation of the experiment was carried out by an MCNPX [40] calculation, using the cross section predicted by the ENDF-VI/B library [41, 42]. First, the code simulated elastic neutron scattering using a point target of ^{208}Pb. The second step was to simulate the reaction using a lead cylinder of the actual size of the experiment. The two angular distributions obtained were compared and correction factors could be calculated from the ratio of the two simulations. Finally, the data on ^{208}Pb were corrected for the content of ^{206}Pb, see Paper I fpr details.

4.2 Experimental uncertainties

Since the purpose of the present experiment has been to obtain a set of relative differential cross section data, which is finally normalized using previously known information, only uncertainties that affect the shape of the angular distribution are of importance.

The random error is due to counting statistics and includes contributions from the background subtraction. It varies significantly with scattering angle, due to the steepness of the cross sections.

The Monte Carlo simulation for correction of multiple scattering, adds a statistical error to the point-to-point uncertainty. The total statistical errors,

including both these contributions, are calculated in the program and given as output together with the corrected angular distribution.

The correction (< 6 %) for the contribution from the low-energy continuum of the ^{7}Li(p,n) spectrum to the *np* scattering peak introduces a systematic uncertainty that varies with peak width and is therefore different for each CsI crystal due to their individual energy resolutions.

For nuclei like ^{208}Pb which have a pronounced angular dependence for the elastic scattering differential cross section, small uncertainties in the angular information can produce significant uncertainties in the result. The effect is present also for iron and yttrium but to a smaller extent. The angular uncertainties in the present experiments are dominated by the incomplete knowledge of the positions of the target and the drift chambers. Both these are known to slightly better than 1 mm, resulting in an angular uncertainty of about 1°. This uncertainty results in an equal shift of all data points produced by the same SCANDAL arm. The drift chambers contain, however, many drift cells, which work as physically independent detectors, each with its own TDC for time recording. Imperfect calibration can produce conversion position errors up to about 0.5 mm, which corresponds to about 0.5° shift of the presumed angle. This uncertainty is randomly distributed among the data points.

4.3 Comparisons with model predictions

4.3.1 Model predictions

Angular distributions of elastic neutron scattering from ^{56}Fe, ^{89}Y and ^{208}Pb are presented in Fig. 4.1, where they are compared with phenomenological (left panel) and microscopic (right panel) optical model predictions. The theoretical curves have been folded with the experimental angular resolution to facilitate comparisons with data. The phenomenological models shown in the left panel are (i) the phenomenological global optical model potential (OMP) by Koning-Delaroche [33] given by solid lines, (ii) a global nucleon-nucleus intermediate-energy potential for ^{208}Pb based on Dirac phenomenology by Kozack and Madland [43], shown as a dotted line, (iii) an OMP calculation by Romain and Delaroche [44] shown as a dash-dotted line and (iv) the cross sections given by the evaluated nuclear data files in the ENDF/B-VI library, Release 6 [41, 42] which are presented with dashed curves. The microscopic potentials shown in the right panel are: (i) by Amos *et al.* [45] presented as solid lines, (ii) a Lane-consistent semi-microscopic OMP by Bauge, Delaroche and Girod [46] shown as dashed lines, (iii) a local, microscopic OMP by Haider and Saliem [47] shown as dotted lines and (iv) a prediction by Crespo and Moro [48] shown as dash-dotted lines. Details on each particular model are given in Paper III.

4.3.2 Comparison with experimental data

Data sets for the three targets were compared with the results of the model predictions described above. The reduced χ^2 (from now on called χ^2) was calculated to investigate the agreement between theory and data. As a normalization error could produce a major χ^2 contribution, it was also tested to re-normalize all theory models to produce a minimum χ^2. It should be noted that none of the predictions contain parameters adjusted to the present experiment.

A detailed comparison between the data and the different models is given in Paper III and, therefore, only an overview will be given here. Visual inspection of the ^{56}Fe, ^{89}Y and ^{208}Pb data and the theory predictions shows that all models, except Crespo-Moro for ^{56}Fe, describe the shape of the experimental angular distributions reasonably well.

χ^2 values were calculated, and for ^{56}Fe the results differed from about 10 to 55. For the normalization test, the four data points at the angles 21.0°, 22.6°, 24.8° and 25.3° were removed. The reason for this is that these data points are in the first minimum, where the formal errors are small, but there are unknown systematic errors due to the multiple scattering correction which we believe are large. If not removed for the re-normalization test, they will dominate the calculation. Re-normalization lowered the χ^2 values significantly (below 10). The required re-normalization to achieve minimum χ^2 ranged from 0.95 to 1.40.

The χ^2 values for ^{89}Y differed from about 1.5 to 5. The re-normalization test required re-normalization ranging from 0.8 to 1.1.

For ^{208}Pb the calculations of χ^2 resulted in values ranging from 3 to 16. For the re-normalization test, the three data points at 13.0°, 14.4° and 17.2° were removed for similar reasons as for the removal of data points for ^{56}Fe. The re-normalization test lowered the χ^2 values for all models, with none exceeding 5. The re-normalizations required ranged from 0.75 to 0.97.

4.4 Comparison with Wick's limit

A basic feature of the optical model is that it establishes a lower limit on the differential elastic scattering cross section at 0° if the total cross section is known. This is often referred to as Wick's limit [34, 35],

$$\frac{d\sigma(0^\circ)}{d\Omega} \geq \left(\frac{\sigma_T}{4\pi\hat{\lambda}}\right)^2. \tag{4.1}$$

For most neutron scattering experiments below 30 MeV, it has been found that the zero-degree cross section is very close to the limit [49, 50] and in the absence of a good experimental normalization this has lead to the suggestion that Wick's limit should be treated as an equality [51]. There is, however, no *a priori* reason why the 0° cross section cannot exceed the limit significantly,

Table 4.1: Wick's limit, $(\sigma_T/4\pi\lambda\!\!\!^{-})^2$, with an error of at most 1 % coming from the determination of the total cross section, and the differential cross sections at 0°. The error for the extrapolated cross section at 0° contains contributions from the normalization procedure as well as the extrapolation to 0°. The ratio is the present data divided by Wick's limit. Predictions from Ref. [52, 53] are also tabulated.

Nucleus	Wick's limit	$d\sigma(0^\circ)/d\Omega$	Ratio	Pred. by [52, 53]
^{12}C	0.77	1.3 ± 0.13	1.70 ± 0.17	-
^{16}O	1.30	2.0 ± 0.2	1.54 ± 0.15	-
^{56}Fe	10.4	12.0 ± 1.3	1.14 ± 0.12	1.22
^{89}Y	20.9	22.7 ± 2.2	1.09 ± 0.10	1.13
^{208}Pb	63.7	60 ± 14	0.95 ± 0.22	1.03

which has also been studied in Ref. [52]. In that work, optical model calculations using the model of Koning-Delaroche were performed for various nuclei and energies. From those data, the deviation from Wick's limit was calculated. It was found that over a wide range of incident energies and target masses, the deviations of the zero-degree differential cross section from Wick's limit are small, at most a few percent. For ^{208}Pb this range is $4-80$ MeV while the corresponding range for ^{89}Y is $10-60$ MeV. The range becomes more narrow, the lighter the nucleus. There is, however, for all nuclei a wide energy range over which the deviation from Wick's limit does not exceed a few percent, while below and above this range the deviations are significant.

In Paper I, the data on ^{208}Pb are in good agreement with Wick's limit while the ^{12}C data overshoot the limit with about 70 %. This has motivated an investigation of the deviation from Wick's limit for our elastic scattering data from ^{16}O (Paper II), ^{56}Fe and ^{89}Y, see Paper III and Table 4.1. It was shown that these data exceed Wick's limit with 54 %, 14 % and 9 %, respectively. Deviations from equality have also been observed in the neutron scattering experiments at 65 MeV [10] and at $65-225$ MeV [11], although not explicitly pointed out by the authors. The deviations are in agreement with our data as well with the calculations performed for Ref. [52]. See Paper III for more details.

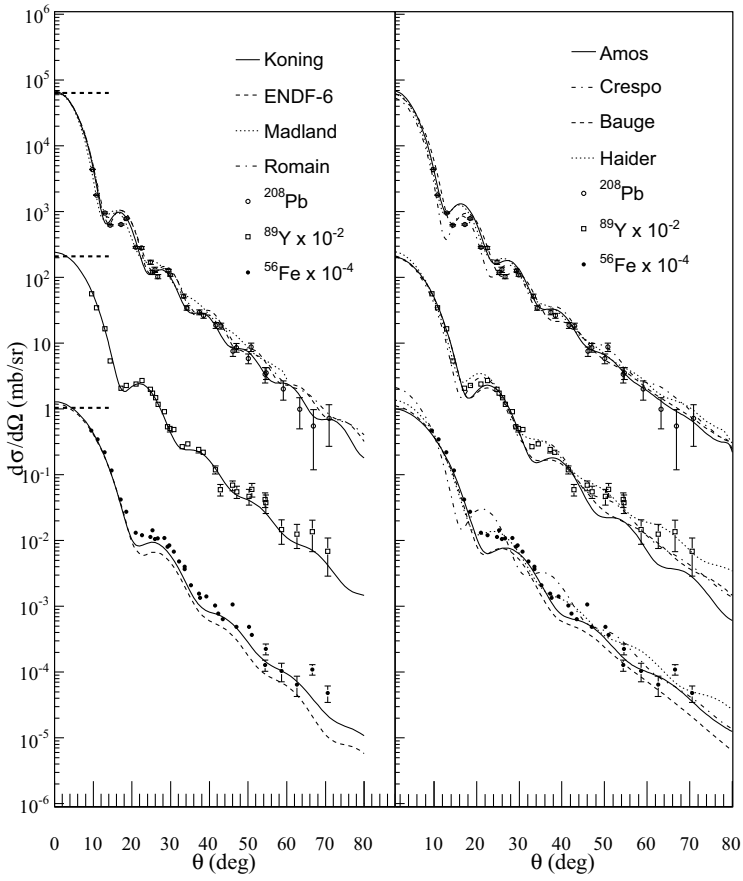

Figure 4.1: Angular distributions of elastic neutron scattering from ^{56}Fe (filled circles), ^{89}Y (squares) and ^{208}Pb (open circles) at 96 MeV incident energy. Only statistical uncertanties are shown. The ^{56}Fe and ^{89}Y data have been multiplied with 10^{-4} and 10^{-2}, respectively. Left panel: predictions by phenomenological optical model potentials (OMP). The thick dotted horizontal lines show Wick's limit for the three nuclei. Right panel: predictions by microscopic OMP. The curves are identified in the text.

5. Inelastic neutron scattering

The previous chapter dealt with the analysis to obtain elastic scattering cross sections from the measurements using the SCANDAL setup. With an extended analysis method, which will be described in this chapter, it was possible to extract data on inelastic cross sections as well. The starting point is the end of chapter 3, where the background-subtracted data have been stored in excitation-energy histograms, one for each angular bin.

5.1 Analysis procedure

The analysis procedure to obtain inelastic cross sections from the SCANDAL data is based on a forward-folding procedure. In short, this means that a physically, reasonable shape of data is assumed and subsequently folded with the response of the experimental setup, to achieve a spectrum which corresponds to the measured data. The outline of this section is the following: first the response function of SCANDAL will be discussed, and second, the forward folding will be described as well as the corrections that need to be applied to obtain the cross sections.

There are three main contributions to the response of the SCANDAL setup. Neutrons converting to protons via *np* scattering produce a single peak in the response spectrum, located at the highest possible energy, i.e., close to the energy of the incident neutron. The carbon content of the converter leads to neutron conversion by ^{12}C(n,p) reactions, resulting in protons at lower energies. The third contribution to the response is provided by the low-energy tail in the incident neutron beam. For more details, see Paper IV.

In Ref. [21] a study of the full response of the SCANDAL setup was performed, using the above information. It was found that it describes the data succesfully. In that study, no time-of-flight (TOF) cut was applied on the incident neutrons, as the exact effect of such a cut cannot be well described analytically. For the present work, this imposes a dilemma. Without a TOF cut, the response function can be reasonably well estimated, but with the drawback that at high excitation energies the contribution of the tail of the response will become very large, which in turn will result in large systematic uncertainties in the folding procedure. If applying a TOF cut, the uncertainties in the folding procedure will be reduced, but the uncertainties in the response are larger.

Instead of using a theoretical approach to determine the response, an experimental response function can be constructed. In principle, it would be possible

to remove the scattering target and place the SCANDAL setup in the neutron beam, i.e., at 0°. Placing the setup in the beam does, however, have other drawbacks. For instance, the beam intensity has to be reduced significantly, and the scaling required in the beam transport could result in various kinds of problems.

This problem can be circumvented by determining the experimental response at small neutron scattering angles, where elastic scattering dominates heavily. Therefore, the proton energy spectrum (and the corresponding excitation-energy spectrum) obtained in SCANDAL at small angles is a good approximation of the response function. With this approach, the combined effect of all the contributions described above are measured. The remaining uncertainty arises from individual effects in the various CsI crystals, and from the energy dependence in the response.

Using this technique, the response at the energy of the incident beam can be determined, but the response at lower energies still has to be modelled. For the present work, we have presumed that the response at lower energies has the same shape as the one at full energy. Behind this strategy is a study of the energy dependence of *np* scattering and the ^{12}C(n,p) reaction. The ratio of these two cross sections stays fairly constant over the relevant energy interval.

As mentioned earlier in the text, forward folding is based on folding a physically reasonable shape of data with the response function. The forward-folded spectrum is compared with experimental data and the parameters of the trial spectrum are adjusted to obtain the best fit. In the present work, two components were used as input to the forward-folding method; a gaussian that describes elastic scattering and for the continuum part of the spectrum, a theory prediction by Kalbach [54, 55, 56, 57] referred to as PRECO. Fig 5.1 shows the differents analysis steps. In the upper panel, the SCANDAL response function is shown. In the second panel, the two components used as input for the forward folding are shown. In the third panel, the measured spectrum is shown as a solid line, the PRECO data folded with the response function is shown as a dashed line and the sum of the two folded components (PRECO and the gaussian) is shown as a dotted line. As can be seen, this gives a fair agreement with the experimental data.

After having folded the components with the resolution of the detector, a spectrum correction was calculated, i.e., the ratio between the input and output in the forward-folding procedure. This correction was multiplied (bin-by-bin) with the experimental spectrum, normalized to keep the elastic peak unchanged.

The final data have to be corrected for the energy dependence of the *np* cross section, as it is closely related to the absolute detection efficiency in SCANDAL, as well as the energy variation of the proton detection efficiency in the CsI crystals. The result can be seen in the lowest panel of Fig 5.1.

5.2 Estimation of experimental uncertainties

Since fairly thick targets have been used, corrections for attenuation and multiple neutron scattering have been performed. These corrections have been based on the behaviour of elastic scattering, i.e., the ground state correction, which is not perfectly correct for inelastic scattering. It turns out, however, that the expected improvement using a correction for multiple scattering for higher excitation-energies is far smaller than the systematic uncertainties in the analysis. Therefore, the original corrections based on elastic scattering have been retained. For more details, see Paper I and III.

We have adopted a procedure in which we simply keep the absolute statistical uncertainty unchanged before and after the folding correction. This can be expected to slightly overestimate the true uncertainties. The systematic uncertainty in the forward-folding procedure has been estimated by varying the input. This was performed by letting the relative intensities of the ground-state gaussian and PRECO vary to obtain optimum agreement with the input spectrum. It was found that the intensities could vary by a few % with no significant difference in the agreement with the experimental spectra. From this it was concluded that the result can vary up to 3% because of the uncertainty in the correction. The systematic uncertainty in the forward-folding procedure has also been studied by using other theory predictions than PRECO to establish the correction. From this study, we have estimated the average systematic uncertainty of the response correction procedure to 5%, see Paper IV.

Other contributions to the systematic uncertainties are due to normalization, multiple scattering and attenuation, uncertainties in the *np* scattering cross sections, and the fact that the H(n,p) and C(n,p) cross sections do not have the exactly same energy dependence. By adding the different contributions of the systematical uncertainties in quadrature, this results in a total systematic uncertainty of 15%. See Paper IV for more details.

5.3 Model interpretation

The data have been compared with different theory models. They have been described in detail in Paper IV and will therefore only be briefly covered here. All theory predictions presented were performed prior to data analysis, i.e., no parameters have been fitted to the present results. The theory predictions shown in Fig. 5.2 are:

- the nuclear-reaction code HMS-ALICE [58], developed by Blann. It has been used for Monte Carlo precompound simulations.
- cross sections of relevance for neutron and proton cancer therapy applications evaluated by Chadwick *et al.* These have been published in ICRU63 [59, 60]
- results from the TALYS code [61].

- the code PRECO [54, 55, 56, 57], developed by Kalbach. It is primarily used for studying preequilibrium reaction mechanisms.
- the microscopic method using quantum molecular dynamics QMD [62]. The method is used to calculate nuclear collision processes in the medium to high-energy region.
- the intra-nuclear cascade (INC) model BRIEFF [63] developed by Duarte.

5.4 Results

Data at 96 MeV incident neutron energy on inelastic neutron emission up to 45 MeV excitation energy in the $26-65^{\circ}$ angular range are presented for ^{56}Fe. Final excitation-energy spectra are presented in Fig. 5.2. The ground state peak, i.e., elastic scattering is prominent at small angles and gets gradually weaker with angle. At the largest angle it is hardly discernible. The continuum appears rather featureless, with the notable exception of a giant resonance structure seen at about 15 MeV excitation energy in the spectra at 26° and 36°. The location of this peak is commensurate with excitation of the well-known isoscalar quadrupole resonance (ISQR). The quality of the data in general, and the lack of data at smaller angles in particular makes it, however, impossible to provide solid evidence for the nature of this structure.

It can be noted that the overall normalization and shape of the theory predictions agrees reasonably well with the experimental data. Comparisons have also been performed with the (n,n'x) measurement at 65 MeV [19], displayed in Fig. 5.3. The shapes are similar and as expected, the double differential cross section is lower for the 96 MeV measurement.

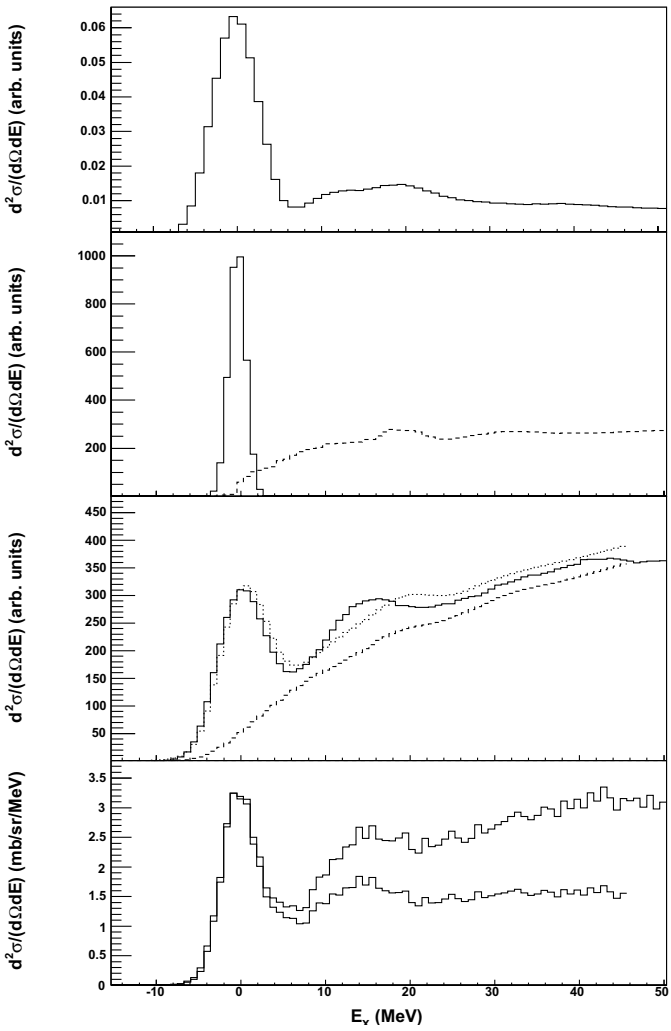

Figure 5.1: The different analysis steps. In the top panel, the response function, i.e., a smoothed spectrum at 9° is displayed. The next panel shows the two components used as input for the forward folding procedure, a gaussian (solid line) and the theory prediction PRECO [54, 55, 56, 57]. The third panel from the top shows the measured spectrum (solid line), the PRECO data folded with the response function (dashed line) and the sum of the two components folded with the response function (dotted line). The bottom panel shows the initial (n,n'x) spectrum before (upper line) and after (lower line) correction.

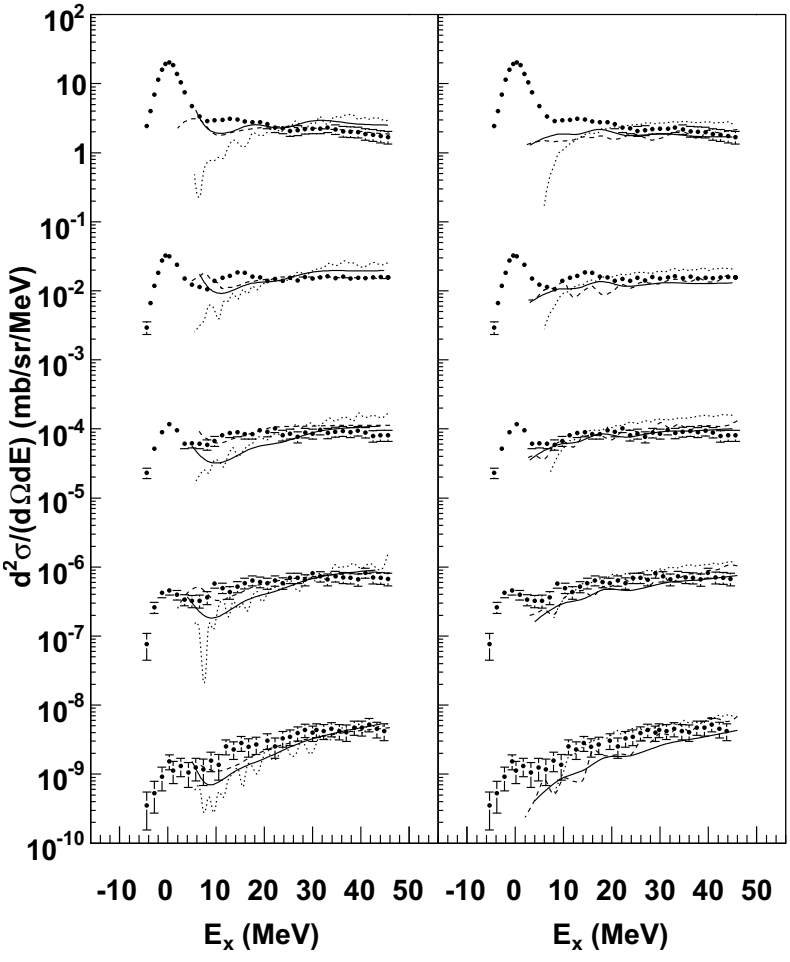

Figure 5.2: Excitation-energy spectra of the (n,n'x) reaction on ^{56}Fe at 96 MeV incident neutron energy. From top to bottom, the data points refer to cross sections obtained at an average angle of 26, 36 (data multiplied by 10^{-2}), 44 (data multiplied by 10^{-4}), 52 (data multiplied by 10^{-6}) and 65 degrees (data multiplied by 10^{-8}). The error bars display the statistical uncertainties. The lines show theory predictions. In the left panel, the solid, dashed and dotted lines refer to predictions by TALYS, ICRU63 and HMS-ALICE, respectively. In the right panel, the solid, dashed and dotted lines refer to predictions by PRECO, QMD and BRIEFF, respectively.

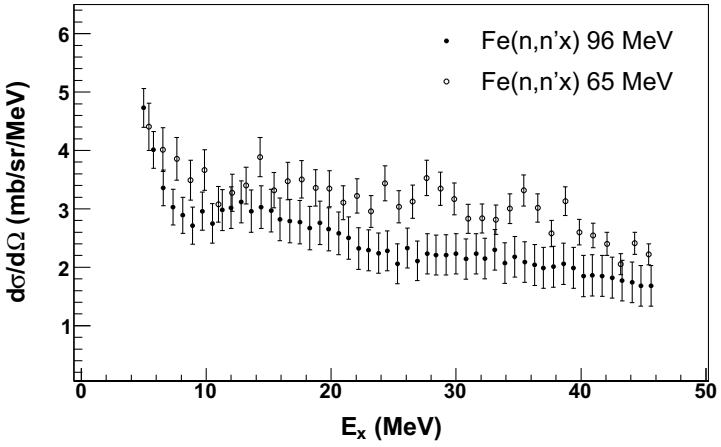

Figure 5.3: Comparison of the (n,n'x) cross section for ^{56}Fe at 65 MeV [19] (open circles) with the (n,n'x) cross sections at 96 MeV (filled circles).

6. Summary, Conclusions and Outlook

In this thesis, cross sections on elastic and inelastic neutron scattering for iron, yttrium and lead at 96 MeV have been presented. The ^{208}Pb data for elastic scattering, see Paper II, have been re-analyzed, resulting in additional angular bins at forward angles, where the cross section is very steep. The new data set supersedes the old one. The overall agreement for ^{56}Fe, ^{89}Y and ^{208}Pb with predictions from theoretical models, both phenomenological and microscopic, is reasonably good. These measurements provide important input to the development of optical models, not the least because of the scarcity of elastic neutron scattering data above 20 MeV.

With a re-fined analysis method, it was possible to extract data on inelastic cross sections from the already existing data, taken with the SCANDAL setup. Data on ^{56}Fe in the angular range $26 - 65^\circ$ and excitation energy range $0 - 45$ MeV have been presented. The data have been compared with theory predictions, which are in reasonable agreement with our results.

A study of the deviation from Wick's limit has been performed. The extrapolated 0° cross section for ^{208}Pb is in agreement with the limit, but large deviations have been found for the lighter nuclei we have studied. These results show the same trend as the previous neutron scattering experiments at 65 MeV [10] and $65 - 225$ MeV [11], and are in agreement with predictions in a recently published paper [52].

The SCANDAL setup is presently being upgraded with thicker CsI crystals, which will allow for measurements at higher energies, i.e., up to 175 MeV which is the maximum energy that can be delivered at the neutron beam facility at the The Svedberg Laboratory. Data on both elastic and inelastic scattering at this energy will certainly be beneficial for the future development of optical models.

7. Summary in Swedish - textad på svenska

"Det har varit roligt och lärorikt,
men jag vet nu att jag varken vill
bli forskare eller kärnfysiker."
Dagboksanteckning 20 aug. 1999 :-)

Har vanliga människor nytta av att kärnreaktioner med neutroner med studeras? Ja, faktiskt. Transmutation av använt kärnbränsle, neutronterapi för cancerbehandling och datorfel i flygplanselektronik är några exempel där kunskap om neutronreaktioner spelar roll. Förutom dessa tillämpningar, så är neutrondata viktiga i grundforskningen, eftersom man kan lära sig mycket om atomkärnors egenskaper från sådana studier.

I den här avhandlingen presenteras nya data för elastisk och inelastisk neutronspridning vid 96 MeV. Dessa data är av stor betydelse eftersom det inte finns särskilt mycket neutrondata över 20 MeV. Neutronspridningsdata används för teoriutveckling av s.k. optiska modeller, som används för att beräkna neutrondata som det inte finns några mätningar för. Detta har man stor nytta av ifall man till exempel ska konstruera en reaktor avsedd för förbränning av kärnavfall eller beräkna stråldos för en cancerbehandling.

Kärnavfallsfrågan har väckt stort intresse över hela världen. Egenskaperna hos det utbrända kärnbränslet gör att det måste förvaras åtskilt från biosfären under lång tid (ca 100 000 år). I många länder, däribland Sverige, finns det planer på att bygga särskilda djupförvar i berggrunden där avfallet ska förvaras inkapslat. En annan möjlighet vore att transmutera kärnbränslet till kortlivade isotoper. Vinsten skulle då bli att man inte behövde bygga ett djupförvar för så långa tider som 100 000 år, utan snarare för ca 1000 år och att risken för skador på lång sikt på biologiskt liv till följd av avfallet skulle kunna reduceras betydligt.

Transmutation av utbränt kärnbränsle bör ske i en reaktor med snabba neutroner. Egenskaperna hos en del av de långlivade isotoperna i avfallet talar för att denna reaktor bör drivas underkritiskt. Det betyder att reaktorn själv inte kan underhålla en kärnreaktion utan neutroner måste ständigt tillföras. Ett exempel på en underkritisk reaktor är det som kallas acceleratordrivet system (ADS). En sådan reaktortyp finns inte idag, men intensiv forskning pågår över hela världen för att kunna utveckla en sådan.

Redan idag är det möjligt att transmutera i laboratorieskala. Alltså behöver inte forskningen koncentreras till att finna de underliggande fysikaliska processerna för transmutation utan till att utveckla detta till ett fungerande system i industriell skala. För att kunna designa en ADS behövs kunskap om alla de kärnreaktioner som kan ske i reaktorn. Att utföra mätningar för alla dessa reaktioner är en omöjlig uppgift både kostnads- och tidsmässigt. Istället

bör man utveckla beräkningsmodeller som kan förutsäga olika kärnreaktioners egenskaper. Ett exempel på en sådan modell är den optiska modellen. En viktig ingrediens för dess utveckling är data på neutronspridning och det är främst där som de neutrondata som presenteras i den här avhandlingen kommer in i bilden.

Experimenten som presenteras i den här avhandlingen har utförts vid The Svedberg Laboratoriet vid Uppsala universitet. En neutronstråle med hög energi (96 MeV) kolliderade med ett strålmål som bestod av järn, yttrium eller bly. Neutronerna som spridits mot atomkärnorna i strålmålet detekterades med hjälp av detektorsystemet SCANDAL (SCAttered Nucleon Detection AssembLy). Därmed kan man bestämma sannolikheten (tvärsnittet) för att en neutron ska spridas mot en viss atomkärna elastiskt eller inelastiskt (vilket betyder att den förlorar en del av sin energi till atomkärnan). Eftersom neutroner är oladdade partiklar som inte kan avge elektriska signaler i en detektor, måste neutronen genomgå en kärnreaktion som skapar en laddad partikel som sedan kan detekteras. I det här experimentet konverteras neutronerna till protoner genom att låta neutronerna krocka med vätekärnor. Sannolikheten för att en neutron ska konverteras till en proton är liten, vilket betyder att man måste köra experimentet lång tid innan man har tillräckligt med statistik för att kunna göra en ordentlig utvärdering av resultaten. För experimenten i den här avhandlingen, så motsvarar varje mätning på en specifik kärna ungefär en veckas experimenttid vid The Svedberglaboratoriet.

I figur 7.1 visas resultaten för elastisk neutronspridning från järn, yttrium och bly. Man kan tydligt se hur sannolikheten för att en neutron ska spridas blir mindre ju större vinkeln är. Eftersom det inte existerar några andra mätningar av hög kvalitet på elastisk spridning över 65 MeV, så har dessa data stor betydelse för teoriutveckling. Som nämnts tidigare är denna teoriutveckling av vikt till exempel vid konstruktion av en framtida ADS-reaktor, men också för att lära sig mer om atomkärnans egenskaper.

Resultat från inelastisk spridning på järn visas i figur 7.2. Våra data jämförs med en liknande mätning fast vid en lägre energi [19]. Man förväntar sig att formen på data ska se ungefär lika ut, men att sannolikheten för inelastisk spridning ska vara lite lägre vid 96 MeV än för 65 MeV, precis som i den här figuren. Även dessa data har stor betydelse för teoriutvecklingen eftersom det inte fanns några data alls tidigare på inelastisk neutronspridning för energier högre än 65 MeV.

Både vad beträffar elastisk och inelastisk neutronspridning flyttar denna avhandling gränsen för kärndata med hög kvalitet. Hittills har neutronspridningsdata med god energiupplösning och rimlig statistisk signifikans producerats upp till 65 MeV. Med föreliggande avhandling vid 96 MeV flyttas gränsen för högkvalitativa data med närmare 50 % uppåt i energi.

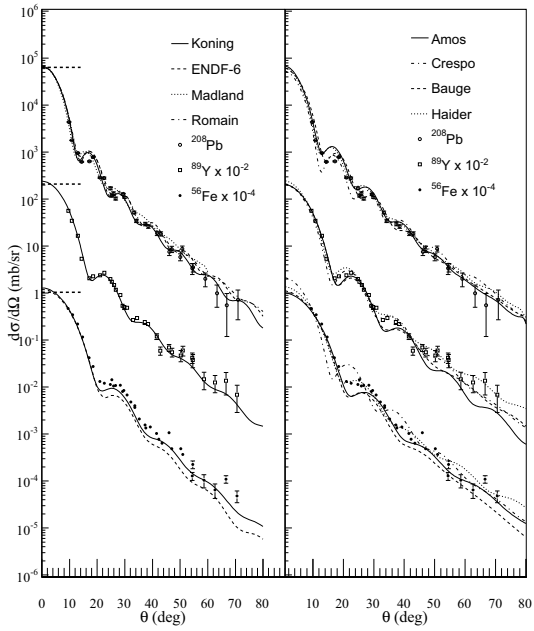

Figure 7.1: Sannolikheten för elastisk neutronspridning vid 96 MeV från järn, yttrium och bly. Data från publikation III jämförs med olika teorimodeller.

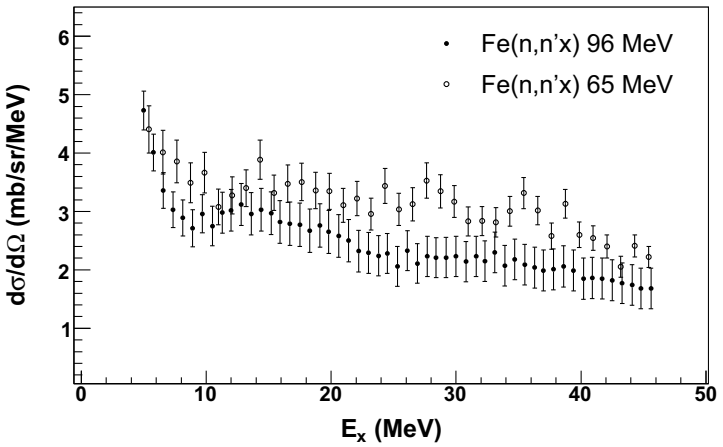

Figure 7.2: Inelastisk spridning av neutroner på järn. Data från publikation IV jämförs här med en liknande mätning, fast vid en lägre energi.

8. Acknowledgements

So, finally it is time to write the acknowledgements. This has been something I have thought of several times during my years as a PhD student. I have thought of interesting and witty expressions. And guess what? They have all escaped my head! Anyway, here I go!

I have learnt and experienced a lot during these years and numerous people have shared their skills and knowledge with me. Without their help I would not have been able to finish this thesis, as experimental nuclear physics is team work.

Firstly, I would like to thank my supervisor, Jan, "Bumpen" Blomgren. Thank you Bumpen for introducing and guiding me through the world of experimental nuclear physics! I greatly appreciate your enthusiasm for my work as well as your open door policy and willingness to discuss my work at all times.

I have been priveleged to have Leif Nilsson as a mentor. His combination of humour, compassion and deep understanding of physics has been crucial for my work. Thank you Leif for your support and encouragement!

Cecilia Gustavsson and Joakim Klug were the senior PhD students when I joined the group. Thank you for introducing me to all the practical stuff that comes with research (= get everything running on the computer as well as understanding the codes), but also for the good company and friendship.

Performing experiments in nuclear physics requires skills in many different areas. My sincere thanks for contributing with everything ranging from a neutron beam to nice coffee breaks go to the staff at the The svedberg Laboratory. Per-Ulf Renberg, Alexander Prokofiev, Lars Einarsson, Olle Jonsson, Torbjörn Hartman, Curt Ekström, Lars Einarsson, Carl-Johan Fridén, Solveig Eriksson, Catharina Åsbjörk and Gun Lundin, it has been a pleasure to work with you!

Anatoly Kolozhvari is acknowledged with thanks for keeping the data-acquisition system running. Your 36-hour shift when we ran the yttrium experiment will be remembered!

The computer systems have been administrated by two real experts: Teresa and Ib you are doing a great job!

I would like to express my sincere gratitude to Michael Österlund for his excellent leadership of the department, and to Susanne Söderberg for her superb administration. Together, the two of you have created a great atmosphere, from which we have all benefited.

My licentiate project was undertaken in collaboration with the Physikalisch-Technische Bundesanstalt (PTB) in Braunschweig, Germany and the Swedish Defense Research Agency (FOI) in Stockholm. There are many people who have contributed to my work, but I would like to especially acknowledge Ralf Nolte (PTB), Dankward Schmidt (PTB), Sylvin Khurana (PTB), Kai Tittelmeier (PTB), Andreas Zimbal (PTB), Angelika (Toll) Kasper (PTB), Katarina Wilhelmsen (FOI), Neda Tooloutalaie (FOI), Klas Elmgren FOI) and Nils Olsson (FOI).

This project would not have been possible without the sponsorship from the Swedish Defense Research Agency (FOI), the Swedish Nuclear Fuel and Waste Management Company, the Swedish Nuclear Power Inspectorate, Ringhals AB, the Swedish Research Council, Forsmark AB, EU and AIM research school.

To the experts in solving computer problems: Pär Olsson (I think that you and Maria should move back to Sweden though), Anders Hjalmarsson and Henrik Jäderström. Thank you!!!

Life in general became much more exciting when my colleague Hans introduced me to "the one". Thank you Hans. I also appreciate that you didn't hesitate to deliver birthday hugs while I was in Germany!

I will certainly miss the members of the "fin-kaffe" gang. Thank you Erik, Henrik, Maria, Carl and Pernilla for being such good friends. And keep going "forward"! :-)

My year as a PhD student included lots of travelling, which I enjoyed very much. I would especially like to thank Mattias Lantz and "Hoa" for fun and interesting company "i främmande land".

During the years as a PhD student, I have been fortunate to have great colleagues. Hoping not to forget anyone, I would like to thank Anna F., Anni, Ane, Christofer, Christine, Göran, Inger, John, Joa, Lele, Lotta, Lovisa, Luca, Marcus, Martin, Matthias W., Nils S., Otas, Pawel, Peter W., Philippe, Riccardo, Sean, Staffan, Stephan, Tobias, Udomrat and Vasily.

For several years I was a member of the choir Schola Cantorum. Thank you "körvänner for all the great trips, parties, concerts, and "fika". Rex Tremenda Majestatis!

En stor kram till Hanna, Henrik (Johansson) och Madde, de bästa vänner man kan ha. A big hug for my friend Laura as well.

Mamma, Pappa, Syster "Grodan" och Robin (postumt), tack för allt stöd och uppmuntran och för att ni är så fantastiska som ni är. Visst är det kul att jag äntligen är klar med "vinklarna"!!! Kram och vink!

Och till sist till min egen familj, Calle och Alexander. Ni är det absolut bästa som finns och jag älskar er otroligt mycket.

Bibliography

[1] R.W. Finlay, W.P. Abfalterer, G. Fink, E. Montei, T. Adami, P.W. Lisowski, G.L. Morgan, and R.C. Haight. *Phys. Rev. C*, 47:237, 1993.

[2] J. Rapaport and E. Sugarbaker. *Ann. Rev. Nucl. Part. Sci*, 44:109, 1994.

[3] W.P. Alford and B.M. Spicer. *Adv. Nucl. Phys.*, 24:1, 1998.

[4] V.G.J. Stoks, R.A.M. Klomp, M.C.M. Rentmeester, and J.J. de Swart. *Phys. Rev. C*, 48:792, 1993.

[5] J. Blomgren, N. Olsson, and J. Rahm. *Phys. Scr.*, T87:33, 2000.

[6] C. Johansson, J. Blomgren, A. Ataç, B. Bergenwall, S. Dangtip, K. Elmgren, A. Hildebrand, O. Jonsson, J. Klug, P. Mermod, P. Nadel-Turonski, L. Nilsson, N. Olsson, S. Pomp, A. V. Prokofiev, P. U. Renberg, U. Tippawan, and M. Österlund. *Phys. Rev. C*, 71:024002, 2005.

[7] R.P. DeVito, S.M. Austin, W. Sterrenburg, and U.E.P. Berg. *Phys. Rev. Lett.*, 47:628, 1981.

[8] R.P. DeVito, S.M. Austin, U.E.P. Berg, R. De Leo, and W.A. Sterrenburg. *Phys. Rev. C*, 28:2530, 1983.

[9] F.P. Brady, T.D. Ford, G.A. Needham, J.L. Romero, C.M. Castaneda, and M.L. Webb. *Nucl. Instr. Meth. A*, 228:89, 1984.

[10] E.L. Hjort, F.P. Brady, J.L. Romero, J.R. Drummond, D.S. Sorenson, J.H. Osborne, B. McEachern, and L.F. Hansen. *Phys. Rev. C*, 50:275, 1994.

[11] J.H. Osborne, F.P. Brady, J.L. Romero, J.L. Ullman, D.S. Sorensson, N.S.P. King, R.C. Haight, J. Rapaport, R.W. Finlay, A. Ling, E. Bauge, J.P. Delaroche, and A.J. Koning. *Phys. Rev. C*, 70:054613, 2004.

[12] M. Ibaraki, M. Baba, T. Miura, Y. Nauchi, Y. Hirasawa, N. Hirakawa, H. Nakashima, S. Meigo, O. Iwamoto, and S. Tanaka. *J. Nucl. Sci. Technol., Suppl.*, 1:683, 2000.

[13] M. Baba, M. Ibaraki, T. Miura, T. Aoki, Y. Hirasawa, H. Nakashima, S. Meigo, and S. Tanaka. *J. Nucl. Sci. Technol., Suppl.*, 2:204, 2002.

[14] A. Bratenahl, S. Fernbach, R.H. Hildebrand, C.E. Leith, and B.J. Moyer. *Phys. Rev.*, 77:597, 1950.

[15] G.L. Salmon. *Nucl. Phys.*, 21:15, 1960.

[16] C.P. van Zyl, R.G.P. Voss, and R. Wilson. *Phil. Mag.*, 1:1003, 1956.

[17] R.S. Harding. *Phys. Rev.*, 111:1164, 1958.

[18] A. Ashmore, D.S. Mather, and S.K. Sen. *Proc. Phys. Soc. A*, 71:552, 1957.

[19] E.L. Hjort, F.P. Brady, J.R. Drummond, B. McEachern, J.H. Osborne, J.L. Romero, and D.S. Sorenson. *Phys. Rev. C*, 53:237, 1996.

[20] NUDATRA, NUclear DAta for TRAnsmutation. Work package of the EUROTRANS project, EUROpean Research Programme for the TRANSmutation of High Level Nuclear Waste in an Accelerator Driven System, EC Contract no. F16W-CT-2004-516520. http://nuklear-server.ka.fzk.de/eurotrans/.

[21] J. Klug, J. Blomgren, A. Ataç, B. Bergenwall, S. Dangtip, K. Elmgren, C. Johansson, N. Olsson, S. Pomp, A.V. Prokofiev, J. Rahm, U. Tippawan, O. Jonsson, L. Nilsson, P.-U. Renberg, P. Nadel-Turonski, A Ringbom, A. Oberstedt, F. Tovesson, V. Blideanu, C. Le Brun, J.F. Lecolley, F.R. Lecolley, M. Louvel, N. Marie, C. Schweitzer, C. Varignon, Ph. Eudes, F. Haddad, M. Kerveno, T. Kirchner, C. Lebrun, L. Stuttgé, I. Slypen, R. Smirnov, A. Michel, S. Neumann, and U Herpers. *Nucl. Instr. Meth. A*, 489:282, 2002.

[22] I. Sagrado Garcia. PhD thesis, Université de Caen, France, 2006.

[23] I. Sagrado Garcia, G. Ban, V. Blideanu, J. Blomgren, P. Eudes, J.M. Fontbonne, Y. Foucher, A. Guertin, F. Haddad, L. Hay, A. Hildebrand, G. Iltis, C. Le Brun, F.R. Lecolley, J.F. Lecolley, J.L. Lecouey, T. Lefort, N. Marie, N. Olsson, S. Pomp, M. Österlund, A. Prokofiev, and J.C. Steckmeyer. In *Proceedings of International workshop on Fast Neutron Detectors and Applications*, Cape Town, South Africa, 2006. http://pos.sissa.it/.

[24] G. Ban, J.M. Fontbonne, G. Iltis, F.R. Lecolley, J.F. Lecolley, J.L. Lecouey, T. Lefort, N. Marie, I. Sagrado Garcia, J.C. Steckmeyer, C. Le Brun, J. Blomgren, A. Öhrn, P. Mermod, N. Olsson, S. Pomp, M. Österlund, A. Prokofiev, M. Fallot, Y. Foucher, A. Guertin, F. Haddad, and M. Vatré. Neutron emission spectrum measurements in the 1-100 mev energy range. Submitted to Nucl. Instr. Meth. Phys. Res. A.

[25] P.-E. Ahlström, S. Andersson, C. Ekberg, J.-O. Liljenzin, M. Nilsson, G. Skarnemark, J. Blomgren, M. Eriksson, W. Gudowski, P. Seltborg, J. Wallenius, and B.R. Sehgal. Partitioning and transmutation current developments - 2004. Technical Report TR-04-15, Swedish Nuclear Fuel and Waste Management, 2004. http://www.skb.se.

[26] A. Wambersie, P. Pihet, and H.G. Menzel. *Radiat. Prot. Dosim.*, 31:421, 1990.

[27] M. Tubiana, J. Dutreix, and A. Wambersie. *Introduction to Radiobiology*. Taylor & Francis, 1990.

[28] H.H.K. Tang. *IBM J. Res. Develop.*, 40:91, 1996.

[29] J. Blomgren, B. Granbom, T. Granlund, and N. Olsson. *Mat. Res. Soc. Bull.*, 28:121, 2003.

[30] Kenneth S. Krane. *Introductory Nuclear Physics*. John Wiley & Sons, Inc., 1988.

[31] G.R. Satchler. *Introduction to Nuclear Reactions*. Oxford University Press, 2nd edition, 1990.

[32] Figure downloaded from http://www.wikimedia.org, Wikimedia commons.

[33] A.J. Koning and J.P. Delaroche. *Nucl. Phys. A*, 713:231, 2003.

[34] G.S. Wick. *Atti R. Accad. Naz. Lincei, Mem. Cl. Sci. Fis., Mat. Nat.*, 13:1203, 1943.

[35] G.C. Wick. *Phys. Rev.*, 75:1459, 1949.

[36] A.J. Koning, 2008. Private communication.

[37] J. Rahm, J. Blomgren, H. Condé, S. Dangtip, K. Elmgren, N. Olsson, T. Rönnqvist, R. Zorro, A. Ringbom, G. Tibell, O. Jonsson, L. Nilsson, P.-U. Renberg, T.E.O. Ericson, and B. Loiseau. *Phys. Rev. C*, 57:1077, 1998.

[38] R.C. Byrd and W.C. Sailor. *Nucl. Instr. Meth. A*, 264:494, 1989.

[39] B. Holmqvist, B. Gustavsson, and T. Wiedling. *Ark. Fys.*, 34:481, 1967. Later updates: N. Olsson.

[40] L.S. Waters. *MCNPX Users' Manual - Version 2.1.5*. Los Alamos National Laboratory, Nov. 1999. http://mcnp-green.lanl.gov/index.html.

[41] P.F. Rose and C.L. Dunford. Endf-102: Data formats and procedures for the evaluated nuclear data file endf-6. Technical Report BNL-NCS-17541, Ed. 4, Brookhaven National Laboratory, National Nuclear Data Center, Upton, NY, 1991.

[42] V. McLane. Endf201: Endf/b-vi summary documentation. Technical Report BNL-NCS-17541, Ed. 4, Brookhaven National Laboratory, National Nuclear Data Center, Upton, NY, 1996.

[43] R. Kozack and D.G. Madland. *Nucl. Phys. A*, 509:664, 1990.

[44] P. Romain and J.P. Delaroche. In *Proceedings from a Specialists Meeting*, page 167. OECD, Paris, 1997. http://db.nea.fr/html/science/om200/.

[45] K. Amos, P.J. Dortmans, H.V. von Geramb, S. Karataglidis, and J. Raynal. *Adv. Nucl. Phys.*, 25:275, 2000.

[46] E. Bauge, J.P. Delaroche, and M. Girod. *Phys. Rev. C*, 63:024607, 2001.

[47] W. Haider and S.M. Saliem. *J. Phys. G*, 28:1313, 2002.

[48] R. Crespo, R.C. Johnson, and J.A. Tostevin. *Phys. Rev. C*, 46:279, 1992.

[49] N. Olsson, B. Trostell, E. Ramström, B. Holmqvist, and F.S. Dietrich. *Nucl. Phys. A*, 472:237, 1987.

[50] J.H. Coon, R.W. Davis, H.E. Felthauser, and D.B. Nicodemus. *Phys. Rev.*, 111:250, 1958.

[51] P.E. Hodgson. *The Optical Model of Elastic Scattering*. Oxford University Press, 1963. p.34.

[52] F.S. Dietrich, J.D. Anderson, R.W. Bauer, and S.M. Grimes. *Phys. Rev. C*, 68:064608, 2003.

[53] F.S. Dietrich, 2007. Private communication.

[54] C. Kalbach. *J. Phys. G: Nucl. Part. Phys.*, 21:1519, 1995.

[55] C. Kalbach. *Phys. Rev. C*, 69:014605, 2004.

[56] C. Kalbach. *Phys. Rev. C*, 72:0246207, 2005.

[57] C. Kalbach. *Phys. Rev. C*, 73:024614, 2006.

[58] M. Blann. *Phys. Rev. C*, 54:1341, 1996.

[59] Icru report 63, nuclear data for neutron and proton radiotherapy and for radiation protection, 2000.

[60] M.B. Chadwick, P.G. Young, S. Chiba, S. Frankles, H.G. Hughes, A.J. Koning, R.C. Little, R.E. MacFarlane, R.E. Prael, and L.S. Waters. *Nucl. Sci. Eng.*, 131:293, 1999.

[61] A.J. Koning, S. Hilaire, and M.C. Duijvestijn. In *Proceedings of Int. Conf. on Nuclear Data for Science and Technology; AIP Conference Proceedings*, volume 769, page 1154, Santa Fe, USA, 2005. www.talys.eu.

[62] J. Aichelin. *Phys. Rev.*, 203:233, 1991. And references therein.

[63] H. Duarte. *Phys. Rev. C*, 75:024611, 2007.

Acta Universitatis Upsaliensis

Digital Comprehensive Summaries of Uppsala Dissertations from the Faculty of Science and Technology 389

Editor: The Dean of the Faculty of Science and Technology

A doctoral dissertation from the Faculty of Science and Technology, Uppsala University, is usually a summary of a number of papers. A few copies of the complete dissertation are kept at major Swedish research libraries, while the summary alone is distributed internationally through the series Digital Comprehensive Summaries of Uppsala Dissertations from the Faculty of Science and Technology. (Prior to January, 2005, the series was published under the title "Comprehensive Summaries of Uppsala Dissertations from the Faculty of Science and Technology".)

Distribution: publications.uu.se
urn:nbn:se:uu:diva-8425

ACTA
UNIVERSITATIS
UPSALIENSIS
UPPSALA
2008